

A Metal-Organic Framework with Optimized Open Metal Sites and Pore Spaces for High Methane Storage at Room Temperature

Zhiyong Guo, Hui Wu, Srinivas Gadipelli, Tengbiao Liao, Yaming Zhou, Shengchang Xiang, Zhenxia Chen, Yongtai Yang, Wei Zhou,* Michael O'Keeffe and Banglin Chen*

((Dedication----optional))

Porous metal-organic frameworks (MOFs) have been emerging as very important functional materials for gas storage, separation, heterogeneous catalysis, sensing and biological imaging.¹ One of the very unique features of such porous MOFs is that the pores can be readily tuned by the deliberate control of framework topologies and framework interpenetration, the usage of diverse metal-containing secondary building blocks, and the incorporation of different organic linkers.²⁻⁸ In fact, quite a large number of porous MOFs have been produced over the past two decades with the pores ranging from 2 to 50 Å; and the superior BET (and Langmuir) surface areas up to 6240 (10,400) m²/g.⁹

To make use of the pore space as the nano-containers, the porous

MOFs have been revealed as the very promising media for gas storage of H₂, CH₄, CO₂, C₂H₂ and many others. Highly porous MOFs with the large pore space and surface areas apparently favor their high gas storage capacities; however, their weak interactions with gas molecules have limited their high gas storage capacities only at low temperature (for example, 77 K for H₂) and/or high pressure up to 100 bar in order to fully utilize the pore space.⁹ Furthermore, the low framework densities of some extremely porous MOFs have also limited their volumetric gas storage capacities, another important parameter for the practical implementation of such materials. The ideal MOF materials for high volumetric gas storage might be those with moderate porosities while the pore spaces and functional sites can be efficiently utilized for their strong interactions with gas molecules, thus their storage capacities can be maximized at room temperature and lower pressure of 35 bar. Motivated by the effectiveness of the *m*-benzenedicarboxylate groups to construct suitable pores for their efficient gas storage, we recently have developed a new hexacarboxylate organic linker H₆BHB (H₆BHB = 3,3',3'',5,5',5''-benzene-1,3,5-triyl-hexabenzic acid).¹⁰ The self-assembly of this BHB linker with the paddle-wheel Cu₂(COO)₄ SBUs led to the formation of a metal-organic framework Cu₃(BHB) (we term UTSA-20; UTSA = University of Texas at San Antonio) with the novel *trinodal* (3,3,4) net of *zyg* topology. The optimized open copper sites and pore spaces within UTSA-20 has enabled them to be fully utilized for methane storage, highlighting UTSA-20 as the material with the highest methane storage density (0.222 g/cm³) at room temperature and 35 bar. The overall absolute volumetric methane storage of 195 cm³/cm³ has featured UTSA-20 as the very few MOFs surpassing the DOE methane storage target of 180 cm³/cm³ at room temperature and 35 bar.¹¹

UTSA-20 was synthesized by the solvothermal reaction of H₆BHB (10 mg, 0.018 mmol) and Cu(NO₃)₂·2.5H₂O (20 mg, 0.086 mmol) in *N,N*-dimethylformamide (DMF) (1.5 ml) with addition of 2 drops of HBF₄ at 65 °C for 48 hrs to give green small block shaped crystals (15.8 mg, 69% yield based on H₆BHB). The compound was formulated as Cu₃(BHB)(H₂O)₃·(DMF)₆(H₂O)_{2.5} by elemental microanalysis.¹²

The acetone-exchanged UTSA-20 was activated at 120 °C for 24 hrs under high vacuum for powder X-ray diffraction and gas sorption studies. As shown in Figure S1, the activated UTSA-20 exhibits a well resolved PXRD pattern which has allowed us to refine the structure by Rietveld refinement. As expected, the *in situ* formed paddle-wheel Cu₂(CO₂)₄ SBUs are bridged by the hexadentate organic linkers BHB to construct a three-dimensional porous MOF of novel *trinodal* (3,3,4) net of *zyg* topology, consisting of two kinds of 3-coordinated nodes, shown as blue and green triangular, and a 4-coordinated node of the paddle-wheel Cu₂(CO₂)₄ cluster,

[*] Dr. Z.-Y. Guo, Dr. S.-C. Xiang, Prof. Dr. B. Chen
Department of Chemistry
University of Texas at San Antonio
One UTSA Circle, San Antonio, Texas 78249-0698
Fax: (+1)-210-458-7428
E-mail: banglin.chen@utsa.edu
Homepage: <http://www.utsa.edu/chem/chen.html>

Dr. H. Wu, Dr. S. Gadipelli, Dr. W. Zhou
NIST Center for Neutron Research,
Gaithersburg, Maryland 20899-6100 and Department of
Materials Science and Engineering, University of Maryland,
College Park, Maryland 20742
E-mail: wei.zhou@nist.edu

Prof. Dr. Y.-M. Zhou, T. Liao, Dr. Z. Chen, Y. Yang
Department of Chemistry
Fudan University, Shanghai, P. R. China 200433

Prof. Dr. M. O'Keeffe
Department of Chemistry and Biochemistry
Arizona State University
Tempe, Arizona 85287

[**] This work was supported by the Award CHE 0718281 from the NSF and AX-1730 from Welch Foundation (BC). Work at NIST was partially supported by the Office of Energy Efficiency and Renewable Energy through the Hydrogen Sorption Center of Excellence. This manuscript was prepared under cooperative agreement 70NANB7H6178 from NIST, U.S. Department of Commerce. The statements, findings, conclusions and recommendations are those of the author(s) and do not necessarily reflect the view of NIST or the U.S. Department of Commerce.

Supporting information for this article is available on the WWW under <http://www.angewandte.org> or from the author.



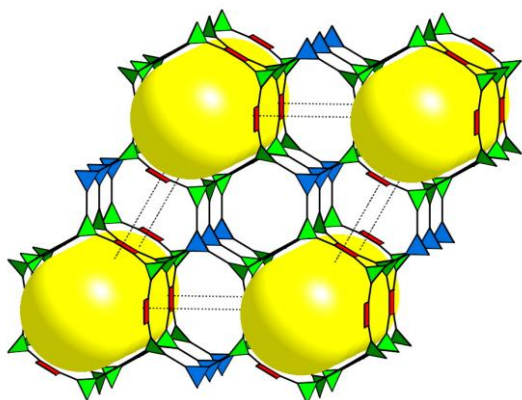


Figure 1. The crystal structure of UTSA-20 consisting of two types of 3-coordinated nodes (blue and green triangular) from BHB linkers and the 4-coordinated node of the paddle-wheel $\text{Cu}_2(\text{CO}_2)_4$ cluster (red square) to form a novel *trindal* (3,3,4) net of *zyg* topology.

shown as a red square planar (Figure 1). Such a novel *zyg* net is significantly different from the *ntt* one constructed from the $\text{Cu}_2(\text{CO}_2)_4$ clusters and larger hexadentate organic linkers mainly because the four benzene rings within BHB are tilted with each other and not coplanar because of the constrain of the crystal structure (Figure S2-3).²⁻⁴ There exists 1D rectangular pores of about $3.4 \times 4.8 \text{ \AA}$ and 1D cylinders of 8.5 \AA in diameter along the *c* axis with the open copper sites exposed to the pores for their potential binding and storage of gas molecules. The total accessible free volume is 3471.0 \AA^3 (63.0 %) of the unit volume 5512.9 \AA^3 .

As shown in Figure 2a, UTSA-20 exhibits type I reversible sorption isotherm and takes up N_2 of $402 \text{ cm}^3/\text{g}$ at 77 K and 1 bar, featuring Langmuir and BET surface area of 1784 and $1156 \text{ m}^2/\text{g}$, respectively. Such porosity is moderate which is even lower than those of HKUST-1 and MOF-505, the two less porous 3D MOFs among those constructed from *m*-benzenedicarboxylate moieties and paddle-wheel $\text{Cu}_2(\text{CO}_2)_4$ clusters.⁸ The high density of open copper sites and small pores are favorable to the high hydrogen storage of 2.9 wt% at 77 K and 1 bar (Figure S4); however, the moderate surface areas apparently have limited its hydrogen uptake of 4.1 wt% at 77 K and 15 bar (Figure S5). The most significant feature is that the optimized open copper sites and pore spaces within UTSA-20 have enabled the pore spaces fully utilized for methane storage. The methane storage density at 150 K and 5 bar can reach to $0.376 \text{ g}/\text{cm}^3$, which is 89% of that of liquid methane ($0.423 \text{ g}/\text{cm}^3$). The methane storage density in UTSA-20 is $0.222 \text{ g}/\text{cm}^3$ at 300 K and 35 bar, which is almost the same as the density of the compressed methane at 300 K and 340 bar, highlighting UTSA-20 as the porous material with the highest methane storage density at 300 K and 35 bar.¹³⁻²² The comparison of UTSA-20 and some previously reported MOFs for their methane storage is shown in Table 1. The efficient usage of the pore spaces contribute to the high volumetric methane storage capacity of UTSA-20 of $178 \text{ cm}^3/\text{cm}^3$ at 300 K and 35 bar (Figure 2), which is slightly lower than the two best MOFs for the volumetric methane storage of about $190 \text{ cm}^3/\text{cm}^3$.²³ The overall absolute volumetric methane storage capacity is $195 \text{ cm}^3/\text{cm}^3$ which has surpassed the DOE standard ($180 \text{ cm}^3/\text{cm}^3$) of porous materials for methane storage at ambient temperature and 35 bar (Figure S6). The optimized open copper sites and pore spaces have also enabled the high volumetric carbon dioxide storage

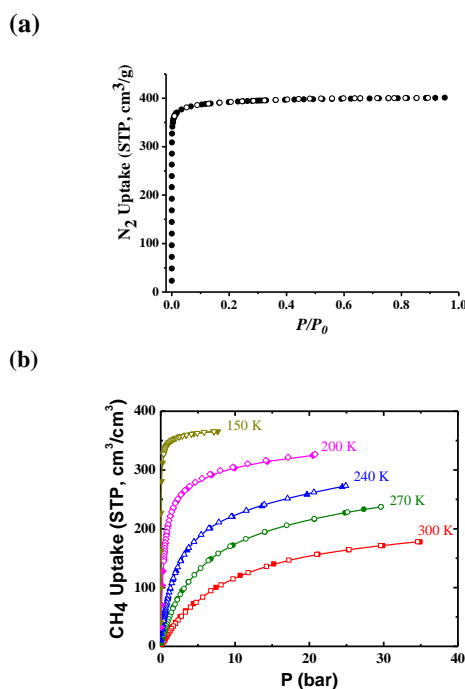


Figure 2. (a) Nitrogen sorption isotherm at 77 K and (b) variable temperature dependent high pressure excess methane sorption isotherms of UTSA-20.

of UTSA-20 ($301 \text{ cm}^3/\text{cm}^3$), which is comparable to those highly porous MOFs of much larger surfaces areas (MIL-101 ($5900 \text{ m}^2/\text{g}$), $300 \text{ cm}^3/\text{cm}^3$; MOF-177 ($5640 \text{ m}^2/\text{g}$), $323 \text{ cm}^3/\text{cm}^3$),²⁴ highlighting the very few porous MOFs whose volumetric carbon dioxide storage capacities are over $300 \text{ cm}^3/\text{cm}^3$ at room temperature and 35 bar (Figure S7 and Table S1).

Table 1. The comparison of UTSA-20 and some previously reported MOFs for their methane storage at room temperature and 35 bar.¹³⁻²²

MOFs	Surface areas (m^2/g) ^a	Pore Volume (cm^3/g)	CH_4 uptake $\text{cm}^3(\text{STP})/\text{cm}^3$	Density of adsorbed CH_4 (g/cm^3) ^c
HKUST-1	1502/2216	0.76	160	0.17
$\text{Zn}_2(\text{bdc})_2(\text{dabco})$	1450/2104	0.68	137	0.17
MIL-101c	4230/5900	2.15	100	0.08
PCN-11	1931/2442	0.91	171	0.18
Ni-MOF-74	1033/1520	0.54	190	0.21
PCN-14	1753/2176	0.87	220 ^b	0.21
UTSA-20	1156/1784	0.63	178	0.22
IRMOF-1	3800/4400	1.04	135	0.15
IRMOF-6	2800/3100	0.92	155	0.19
$\text{CuSiF}_6(4,4'$ - $\text{bipy})_2$	1337	0.56	125	0.19
MOF-200	4530/10400	3.59	41	0.04
MOF-205	4460/6170	2.16	93	0.08
MOF-210	6240/10400	3.60	53	0.04

^aBET/Langmuir surface areas; ^b at 290 K; ^c in micropores.

The coverage-dependent adsorption enthalpies of UTSA-20 to methane were calculated based on virial method,⁸ a well established and reliable methodology from fits of their adsorption isotherms at 273 and 295 K. As shown in Figure S8, UTSA-20 exhibits quite high adsorption enthalpies of CH₄ (23.3 kJ/mol at the zero coverage) which are slightly higher than those MOFs for high density methane storage.²¹

To investigate the methane adsorption and storage mechanism in UTSA-20, we performed detailed computational investigations. Previous studies on the methane storage in other MOFs with dicopper paddle wheel units have well established that the open-Cu site binds CH₄ strongly and is one of the primary methane adsorption sites.²⁵ The same is expected for UTSA-20 since it contains the same open copper units. We note that direct binding of one methane molecule at each Cu site only accounts for a maximal storage capacity of ~89 cm³(STP)/cm³, half of the 178 cm³(STP)/cm³ as measured at RT and 35 bar. To reveal other major CH₄ adsorption sites, we performed Grand Canonical Monte Carlo (GCMC) simulations of methane adsorption in UTSA-20 (with the open-Cu sites preoccupied by methane) using the classical force-field method.²⁶ Simulations were performed at 298 K and various pressures (0.1, 1, 10, and 35 bar). The probability distribution of adsorbed CH₄ was generated from the simulation after the equilibrium stage, and the result obtained at the pressure of 10 bar is shown in Figure 3a as an example. Clearly, the channel-like pore spaces between the parallelly stacked BHB linkers (along the *c*-axis) are heavily populated by CH₄ molecules, and we term this site the “linker channel site”. At higher pressure, additional adsorption sites can be found, but they are much weaker and less-defined adsorption sites. We note that full saturation of the open-Cu site and the linker channel site can generate a methane capacity of about 162 cm³(STP)/cm³, which is approximately 90% of the experimental uptake at 298 K and 35 bar. The remaining storage capacity can be easily provided by those additional secondary adsorption sites.

We further discussed the energy aspect of the adsorption of methane on the two major sites. The static methane binding energies (E_B) were calculated based on density-functional theory²⁷ with a semiempirical correction²⁸ for dispersive interactions (DFT-D). For the open-Cu site and the linker channel site, calculated E_B 's are 21.6 and 23.5 kJ/mol, respectively, in reasonable agreement with the above experimental Q_{st} values. Interestingly, the methane binding at the linker channel site is even stronger than that at the open-Cu site. While the methane binding on the open-Cu site was known to partly due to the enhanced electrostatic interaction between the metal ion and the slightly polarized methane molecule, the methane interaction with the framework at the linker channel site is mainly of van der Waals (vdW) nature. We found that the size of the linker channel pore is just “appropriate” to enable the methane molecule interact with two BHB linkers simultaneously. To further illustrate this, in Figure 3b, we plot the vdW surface of the UTSA-20 channel pores along with the adsorbed methane at the linker channel sites. Clearly, the methane molecule is “sandwiched” between two BHB linker potential surfaces, which results in enhanced overall interaction. The strong interactions of the both open copper sites and the linker channel sites with methane gas molecules have enabled the pore spaces within UTSA-20 fully utilized for methane storage, thus featuring UTSA-20 as the porous MOF with the highest methane storage densities (Figure S9).

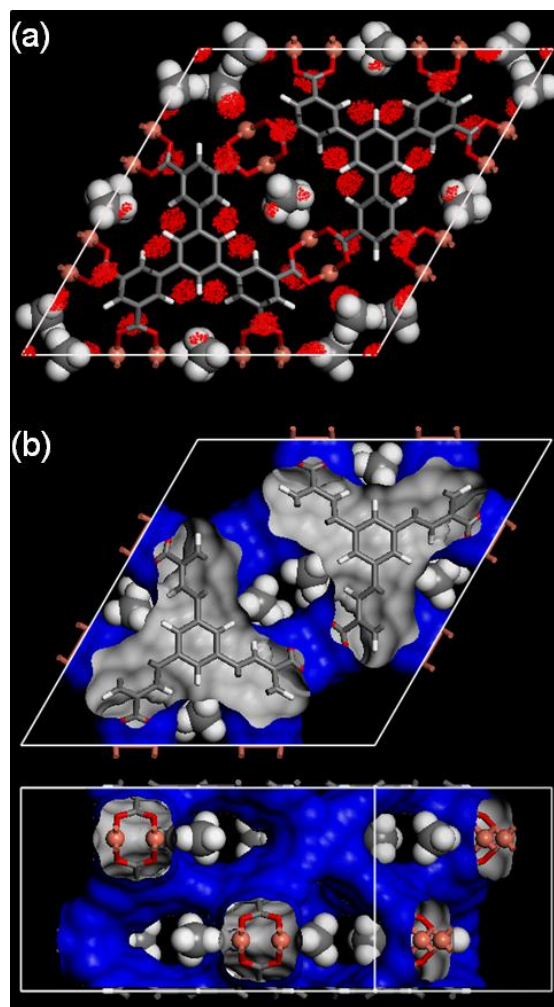


Figure 3. (a) Probability distribution of the CH₄ center of mass in UTSA-20 ([0 0 1] view), obtained from GCMC simulation at 298 K and 10 bar. Note that the open-Cu site is preoccupied with CH₄ molecules in order to focus our effort on the search of other strong methane adsorption sites; (b) The vdW surface of the interconnected channel pores in UTSA-20, with adsorbed methane at the linker channel site. The channel width along the *c*-axis is in good match with the adsorbed methane molecules, leading to enhanced vdW interaction.

In summary, we realized a 3D porous metal-organic framework (UTSA-20) of the novel *trinodal* (3,3,4) net of *zyg* topology by the self-assembly of the nonlinear hexacarboxylate (BHB) with the paddle-wheel Cu₂(COO)₄ cluster. Although its porosity as demonstrated by its surface area is moderate and much lower than most of highly porous MOFs, the optimized open copper sites and pore spaces within UTSA-20 has enabled the pore spaces fully utilized for methane storage, featuring UTSA-20 as the material with the highest methane storage density (0.222 g/cm³), and the third porous MOF whose absolute volumetric methane storage has surpassed the DOE methane storage target of 180 cm³/cm³ at room temperature and 35 bar. By the immobilization of high density open metal sites and the deliberate control of the pore space for their efficient methane storage, the emerging porous MOFs are envisioned to be very promising media for methane and nature gas storage, and then implemented to our daily usage of methane-driven automobiles in the near future.

Experimental Section

Powder X-ray Crystallography: Phase identification was conducted on samples sealed in glass capillaries, using a Rigaku X-ray diffractometer with a Cu K α source. Data were collected over 14 h at room temperature in the 2 θ range of 5–60° with a step size of 0.02°. The X-ray diffraction (XRD) reflections of the as-synthesized UTSA-20 samples can be indexed using a hexagonal cell with $a = 21.971$ Å and $c = 13.547$ Å. Evaluation of the systematic absences in the XRD pattern indicated the following most possible space groups: $P6_3cm$, $P6_3c2$, $P6_3/mcm$, $P31c$, and $P-3c1$. After activation, the symmetry of the UTSA-20 structure remains unchanged. We then solved the crystal structure using the direct method, and space group was identified as $P6_3/mcm$. Finally, Rietveld refinement was performed on the XRD pattern collected on the activated sample, using the GSAS package. Refinement on the lattice parameters, background, peak profile, as well as the atomic positions of Cu, C and O with constraints applied on C-C and C-O bonds lengths yields the agreement factors of $R_{wp}=0.0811$ and $R_p=0.0644$, which strongly supports the validity of our structure solution. Note that the quality and insensitivity of laboratory XRD data do not allow accurate determination of H atom, and thus the positions of H were estimated from the geometry and the common bond length of C-H. The refined lattice parameters are $a = 22.286(1)$ Å and $c = 12.816(1)$ Å. CCDC-795055 (UTSA-20) contains the supplementary crystallographic data for this paper. These data can be obtained free of charge from The Cambridge Crystallographic Data Centre via www.ccdc.cam.ac.uk/conts/retrieving.html (or from the Cambridge Crystallographic Data Centre, 12 Union Road, Cambridge CB21EZ, UK; fax: (+44)1223-336-033; or deposit@ccdc.cam.ac.uk).

Received: ((will be filled in by the editorial staff))

Published online on ((will be filled in by the editorial staff))

Keywords: Porous Materials ·Molecular Recognition, Open Metal Site, Porous Metal-Organic Frameworks ·Methane Storage

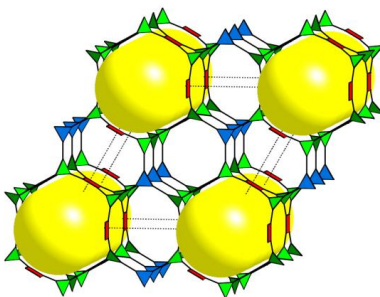
- [1] O. M. Yaghi, M. O'Keeffe, N. W. Ockwig, H. K. Chae, M. Eddaoudi, J. Kim, *Nature* **2003**, *423*, 705; S. Kitagawa, R. Kitaura, S. Noro, *Angew. Chem. Int. Ed.* **2004**, *43*, 2334; M. Dinca, J. R. Long, *Angew. Chem. Int. Ed.* **2008**, *47*, 6766; R. E. Morris, P. S. Wheatley, *Angew. Chem. Int. Ed.* **2008**, *47*, 4966; J. M. Thomas, *Topics in Catalysis*, **2008**, *50*, 98; W. Lin, J. W. Rieter, K. M. L. Taylor, *Angew. Chem. Int. Ed.* **2009**, *48*, 650; L. Ma, C. Abney, W. Lin, *Chem. Soc. Rev.* **2009**, *38*, 1248; B. Chen, S.-C. Xiang, G.-D. Qian, *Acc. Chem. Res.* **2010**, *43*, 1115.
- [2] D. Zhao, D. Yuan, D. Sun and H.-C. Zhou, *J. Am. Chem. Soc.*, **2009**, *131*, 9186.
- [3] Y. Yan, I. Telepeni, S. Yang, X. Lin, W. Kockelmann, A. Dailly, A. J. Blake, W. Lewis, G. S. Walker, D. R. Allan, S. A. Barnett, N. R. Champness and M. Schroder *J. Am. Chem. Soc.* **2010**, *132*, 4092.
- [4] O. K. Farha, A. O. Yazaydin, I. Eryazici, C. D. Malliakas, B. G. Hauser, M. G. Kanatzidis, S. T. Nguyen, R. Q. Snurr and J. T. Hupp, *Nat. Chem.* **2010**, doi:10.1038/nchem.834.
- [5] J. Zhang, T. Wu, S.-M. Chen, P. Feng, X. Bu, *Angew. Chem. Int. Ed.* **2009**, *48*, 3486.
- [6] Y.-B. Zhang, W.-X. Zhang, F.-Y. Feng, J.-P. Zhang, X.-M. Chen, *Angew. Chem. Int. Ed.* **2009**, *48*, 5287.
- [7] A. J. Lan, K. H. Li, H. H. Wu, D. H. Olson, T. J. Emge, W. Ki, M. C. Hong and J. Li, *Angew. Chem. Int. Ed.*, **2009**, *48*, 2334.
- [8] S.-C. Xiang, W. Zhou, J. M. Gallegos, Y. Liu and B. Chen, *J. Am. Chem. Soc.*, **2009**, *131*, 12415; S.-C. Xiang, W. Zhou, Z. Zhang, Y. Liu, B. Chen, *Angew. Chem. Int. Ed.*, **2010**, *49*, 4615.
- [9] H. Furukawa, N. Ko, Y. B. Go, N. Aratani, S. B. Choi, E. Choi, A. O. Yazaydin, R. Q. Snurr, M. O'Keeffe, J. Kim, O. M. Yaghi, *Science*, **2010**, *239*, 424.
- [10] Z. Chen, S.-C. Xiang, T. Liao, Y. Yang, Y.-S. Chen, Y. Zhou, D. Zhao and B. Chen, *Crystal Growth & Design*, **2010**, *10*, 2775.
- [11] Burchell, T.; Rogers, M. *SAE Tech. Pap. Ser.* **2000**, 2000-01-2205.
- [12] Elemental analysis (%) for UTSA-20 (C₄₈H₆₅N₆O_{23.5}Cu₃): calcd: C, 44.60; H, 5.07; N, 6.50%; found: C, 44.36; H, 4.69; N: 6.39%.
- [13] S.-I. Noro, S. Kitagawa, M. Kondo, K. Seki, *Angew. Chem. Int. Ed.* **2000**, *39*, 2081.
- [14] M. Kondo, M. Shimamura, S.-I. Noro, S. Minakoshi, A. Asami, K. Seki, S. Kitagawa, *Chem. Mater.* **2000**, *12*, 1288.
- [15] M. Eddaoudi, J. Kim, N. Rosi, D. Vodak, J. Wachter, M. O'Keeffe, O. M. Yaghi, *Science*, **2002**, *295*, 469.
- [16] S. Ma, D. Sun, J. M. Simmons, C. D. Collier, D. Yuan, H.-C. Zhou, *J. Am. Chem. Soc.* **2008**, *130*, 1012.
- [17] P. L. Llewellyn, S. Bourrelly, C. Serre, A. Vimont, M. Daturi, L. Hamon, G. D. Weireld, J.-S. Chang, D.-Y. Hong, Y. K. Hwang, S. H. Jhung and G. Ferey, *Langmuir* **2008**, *24*, 7245.
- [18] X.-S. Wang, S. Ma, K. Rauch, J. M. Simmons, D. Yuan, X.-S. Wang, T. Yildirim, W. C. Cole, J. J. Lopez, A. DeMeijere, H.-C. Zhou, *Chem. Mater.* **2008**, *20*, 3145.
- [19] H. Wu, W. Zhou, T. Yildirim, *J. Phys. Chem. C* **2009**, *113*, 3029.
- [20] H. Kim, D. G. Samsonenko, S. Das, G.-H. Kim, H.-S. Lee, D. N. Dybtsev, E. A. Berdonosova and K. Kim, *Chem. Asian J.* **2009**, *4*, 886.
- [21] H. Wu, W. Zhou, T. Yildirim, *J. Am. Chem. Soc.* **2009**, *131*, 4995.
- [22] H. Wu, J. M. Simmons, Y. Liu, C. M. Brown, X.-S. Wang, S. Ma, V. K. Peterson, P. D. Southon, C. J. Kepert, H.-C. Zhou, T. Yildirim and W. Zhou, *Chem. Eur. J.* **2010**, *16*, 5205.
- [23] The claim of 220 cm³/cm³ for PCN-14 was carried out at a lower temperature of 290 K. The expected volumetric methane storage capacity is expected to be lower at 300 K.
- [24] A. R. Millward and O. M. Yaghi *J. Am. Chem. Soc.*, **2005**, *127*, 17998.
- [25] W. Zhou, *Chem. Rec.* **2010**, *10*, 200.
- [26] D. Frenkel and B. Smit, *Understanding Molecular Simulation: From Algorithms to Applications*. San Diego: Academic Press, 2002.
- [27] P. Giannozzi, S. Baroni, et al. *J. Phys.: Condens. Matter* **2009**, *21*, 395502.
- [28] Barone, V.; Casarin, M.; Forrer, D.; Pavone, M.; Sambi, M.; Vittadini, A. *J. Comput. Chem.* **2009**, *30*, 934.

Metal-Organic Framework

Z. Guo, H. Wu, S. Gadipelli, T. Liao, Y. Zhou, S.-C. Xiang, Z. Chen, Y. Yang, W. Zhou,* M. O’Keeffe and B. Chen*

Page – Page

A Metal-Organic Framework with Optimized Open Metal Sites and Pore Spaces for High Methane Storage at Room Temperature



The optimized open copper sites and pore spaces within UTSA-20 of the *trinodal* (3,3,4) net has featured UTSA-20 as the material with the highest methane storage density (0.22 g/cm^3), and the few porous MOF ($195 \text{ cm}^3/\text{cm}^3$) surpassing the DOE methane storage target of $180 \text{ cm}^3/\text{cm}^3$ at room temperature and 35 bar.

Supporting Information for the Manuscript

A Metal-Organic Framework with Optimized Open Metal Sites and Pore Spaces for High Methane Storage at Room Temperature

Zhiyong Guo,[†] Hui Wu,[‡] Srinivas Gadipelli,[‡] Tengbiao Liao,[§] Yaming Zhou,[§] Shengchang Xiang,[†] Zhenxia Chen,[§] Yongtai Yang,[§] Wei Zhou,^{*,‡} Michael O'Keeffe[#] and Banglin Chen^{*,†}

Contribution from [†]Department of Chemistry, University of Texas at San Antonio, San Antonio, Texas 78249-0698, [‡]NIST Center for Neutron Research, Gaithersburg, Maryland 20899-6100, [§]Department of Materials Science and Engineering, University of Maryland, College Park, Maryland 20742, [§]Department of Chemistry, Fudan University, Shanghai, P. R. China 200433, and [#]Department of Chemistry and Biochemistry, Arizona State University, Tempe, Arizona 85287

Corresponding authors' email addresses: wei.zhou@nist.gov; banglin.chen@utsa.edu

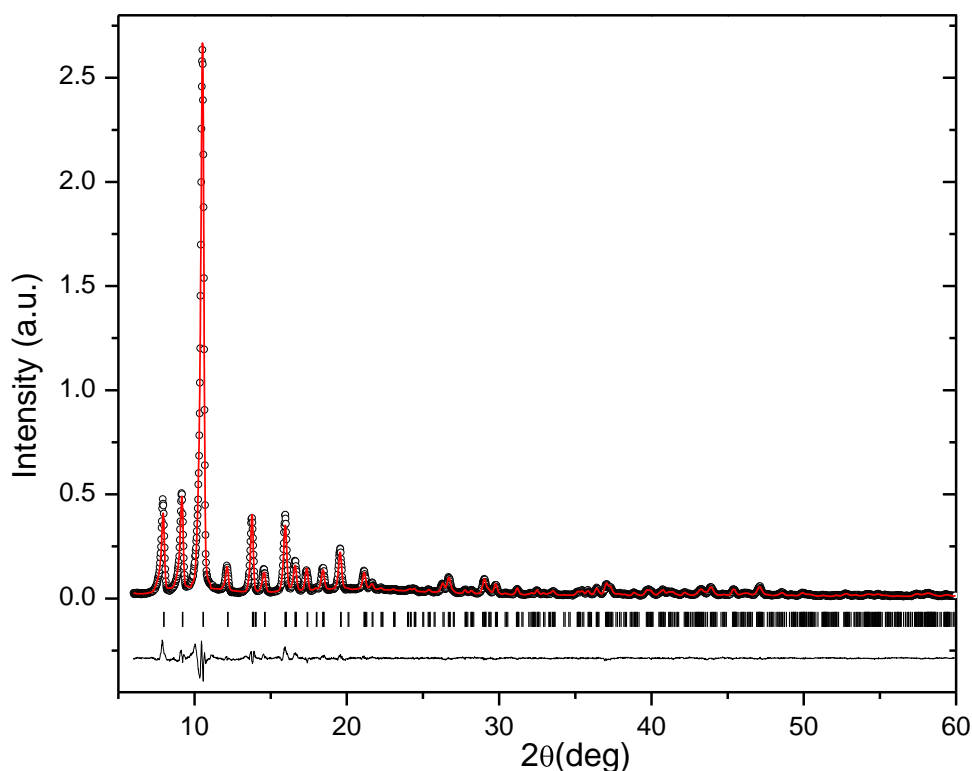


Figure S1 Experimental (circles), fitted (line), and difference (noisy line below observed and calculated patterns) XRD profiles for activated UTSA-20 at 298 K. Vertical bars indicate the calculated positions of Bragg peaks for UTSA-20.

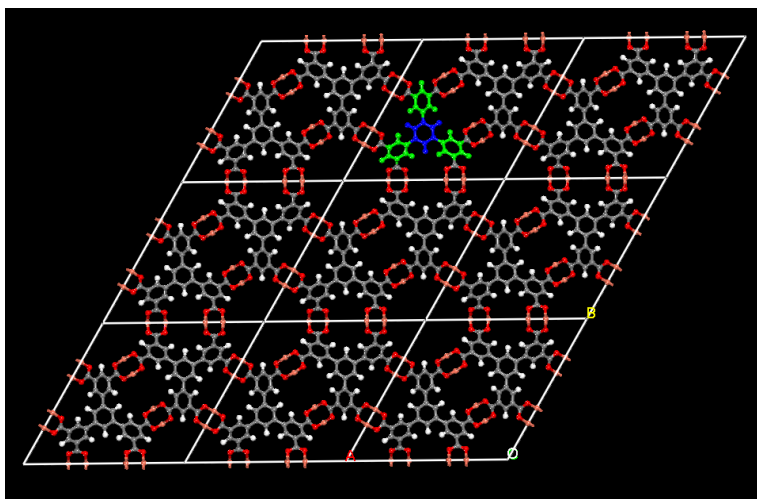


Figure S2 The crystal structure of UTSA-20 viewed along c axis (Color scheme: C, gray; H, white; O, red; Cu, orange. Both the central (blue) and peripheral (green) benzene of BHB organic linker act as the 3-coordinated triangular nodes in its *trinodal* (3,3,4) net of *zyg* topology).

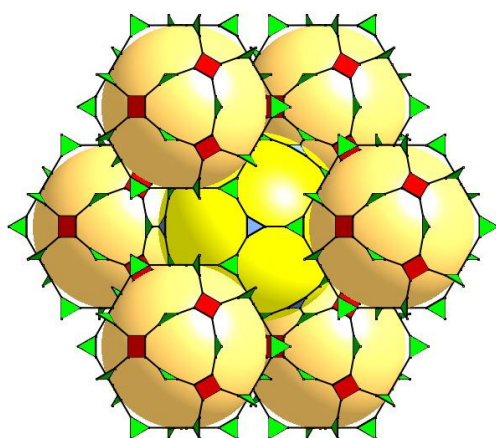


Figure S3 *Ntt* topology of the metal-organic frameworks constructed from paddle-wheel $\text{Cu}_2(\text{COO})_4$ clusters and large planar hexacarboxylates.

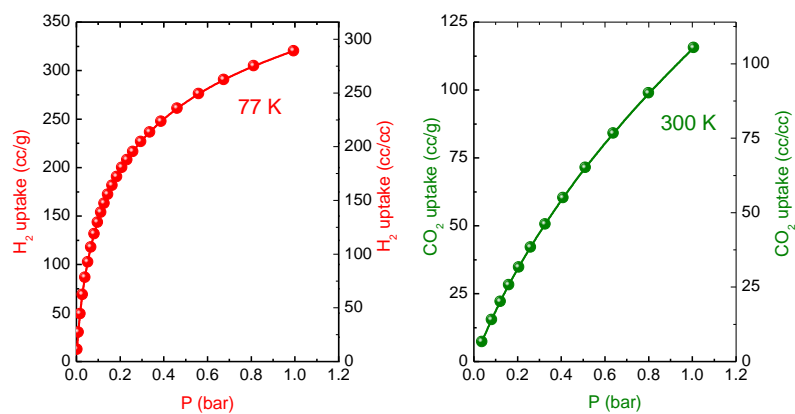


Figure S4 Low pressure (Left) H₂ sorption at 77 K and (right) CO₂ sorption at 300 K.

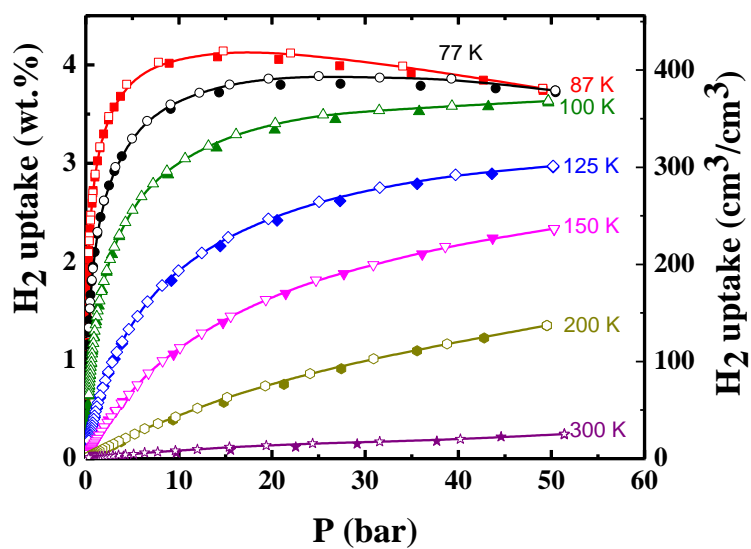


Figure S5 High pressure excess hydrogen sorption isotherms of UTSA-20 at different temperatures.

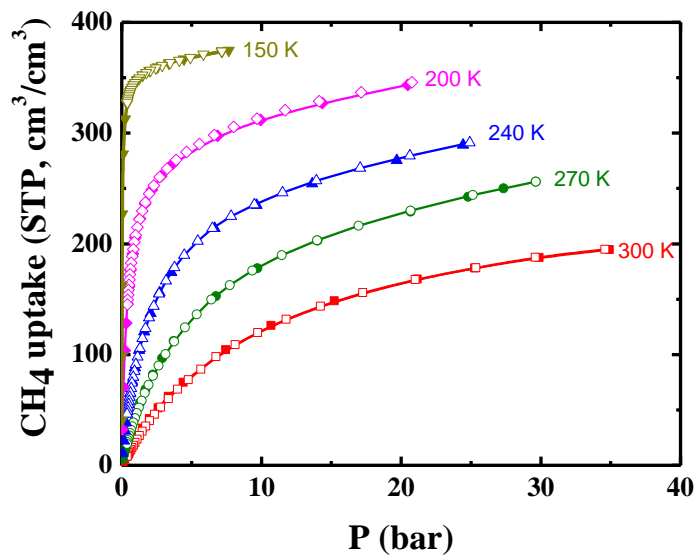


Figure S6 High pressure absolute methane sorption isotherms of UTSA-20 at different temperatures.

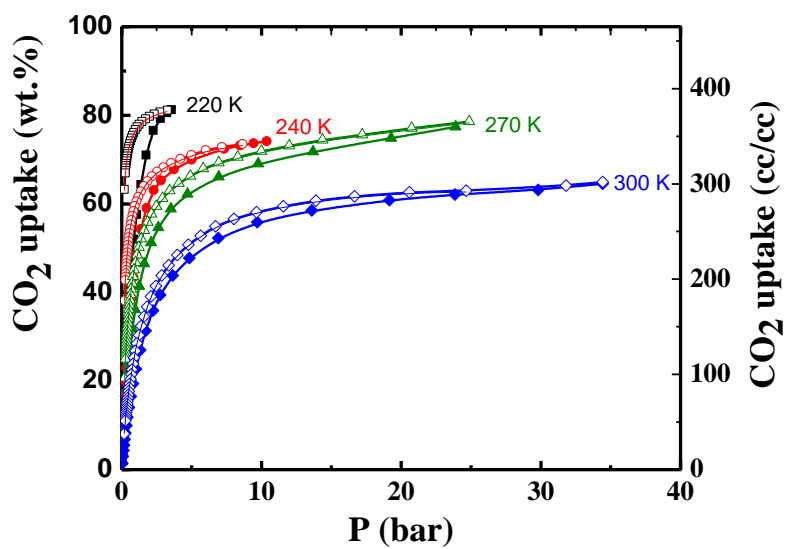


Figure S7 High pressure excess carbon dioxide sorption isotherms of UTSA-20 at different temperatures.

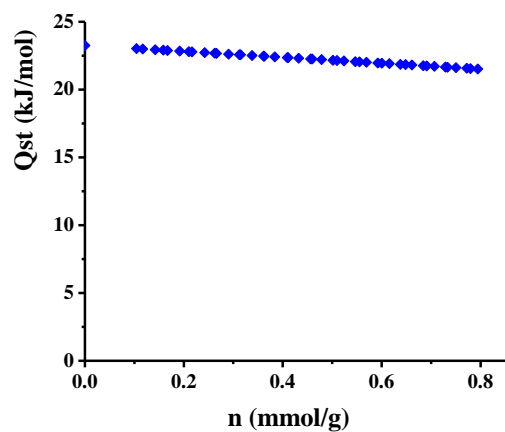


Figure S8 Coverage dependency of the adsorption enthalpies for CH₄ in UTSA-20 calculated from virial fits of their 273 and 295 K sorption isotherms.

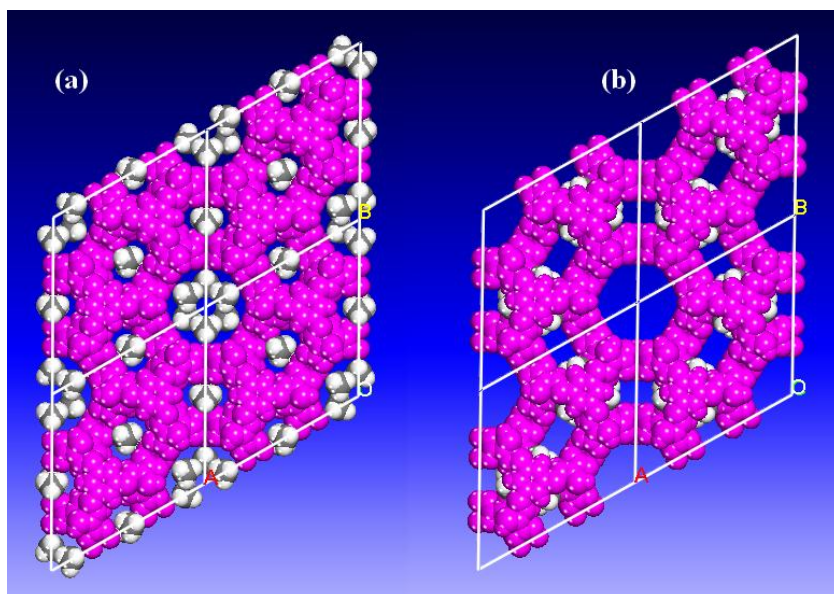


Figure S9 (a) The open copper sites and (b) linker channel sites for high density methane storage in UTSA-20.

Table S1 CO₂ uptake in some examined metal-organic frameworks at room temperature and 35 bar.

	Crystal Density (g/cm ³)	Surface areas (BET/Langmuir) (m ² /g)	Pore volume (cm ³ /g)	Excess CO ₂ uptake (cm ³ /cm ³)
HKUST-1	0.88	1502/2216	0.76	211
MIL-101c	0.44	4230/5900	2.15	300
Ni-MOF-74	1.21	1033/1520	0.54	263
UTSA-20	0.91	1156/1784	0.63	301
IRMOF-1	0.61	3800/4400	1.04	297
IRMOF-6	0.65	2800/3100	0.92	283
MOF-177	0.43	4750/5640	1.59	323
MOF-200	0.22	4530/10400	3.59	226
MOF-205	0.38	4460/6170	2.16	288
MOF-210	0.25	6240/10400	3.60	248

Derivation of the Isothermic Heats of Adsorption: A virial type expression of the following form was used to fit the combined isotherm data for a given material at 295.0 and 273.2 K.¹

$$\ln P = \ln N + 1/T \sum_{i=0}^m a_i N^i + \sum_{i=0}^n b_i N^i \quad (1).$$

Here, P is the pressure expressed in Torr, N is the amount adsorbed in mmol/g, T is the temperature in K, a_i and b_i are virial coefficients, and m , n represents the number of coefficients required to adequately describe the isotherms. The equation was fit using the statistical software package *SPSS* 16.0. m and n were gradually increased until the contribution of extra added a and b coefficients was deemed to be statistically insignificant towards the overall fit, as determined using the average value of the squared deviations from the experimental values was minimized. In all cases, $m \leq 6$ and $n \leq 3$. The values of the virial coefficients a_0 through a_m were then used to calculate the isothermic heat of adsorption using the following expression.

$$Q_{st} = -R \sum_{i=0}^m a_i N^i \quad (2).$$

Here, Q_{st} is the coverage-dependent isothermic heat of adsorption and R is the universal gas constant of 8.3147 J K⁻¹mol⁻¹.

Computational methods:

Grand Canonical Monte Carlo (GCMC) simulation were performed for CH₄ adsorption in UTSA-20, with both the CH₄ molecules and the frameworks treated as rigid bodies. A 2×2×2 supercell was used as the simulation box to ensure the simulation accuracy. 2×10⁷ steps were used for equilibration and additional 2×10⁷ steps were used to calculate the ensemble average of CH₄ adsorption sites and thermodynamic properties. We used the standard universal force field (UFF) to describe the methane-framework interaction and the methane-methane interaction Atomic partial charges derived from first-principles calculation were included in the simulation to account for electrostatic interactions. More technical details of our GCMC simulations can be found in our previous work.

First-principles calculations based on density-functional theory were performed using the PWSCF package. A semiempirical addition of dispersive forces to conventional DFT was included in the calculation to account for vdW interactions between the CH₄ and the framework. We used Vanderbilt-type ultrasoft pseudopotentials and the generalized gradient approximation (GGA) with the Perdew-Burke-Ernzerhof (PBE) exchange correlation. A cutoff energy of 544 eV and a *gamma*-point k sampling were sufficient for the total energy to converge within 0.5 meV/atom. We first optimized the bare UTSA-

20 structure. CH₄ molecules were then introduced to the optimized MOF structure (guided by the GCMC result), followed by a full structural relaxation. To obtain the CH₄ binding energies, a CH₄ molecule placed in a supercell with the same cell dimensions was also relaxed as a reference. The static binding energy was then calculated using: $E_B = [E(\text{MOF}) + nE(\text{CH}_4) - E(\text{MOF} + n\text{CH}_4)]/n$.

References:

1. J. Roswell, O. M. Yaghi, *J. Am. Chem. Soc.* **2006**, *128*, 1304.
2. S. Baroni, A. Dal Corso, S. de Gironcoli, P. Giannozzi, C. Cavazzoni, G. Ballabio, S. Scandolo, G. Chiarotti, P. Focher, A. Pasquarello, K. Laasonen, A. Trave, R. Car, N. Marzari, A. Kokalj, Quantum-ESPRESSO; <http://www.pwscf.org/>.